Journal of Atmospheric and Solar-Terrestrial Physics 73 (2011) 137–145

Contents lists available at ScienceDirect

Journal of Atmospheric and Solar-Terrestrial Physics

journal homepage: www.elsevier.com/locate/jastp

Polar UVI and THEMIS GMAG observations of the ionospheric response to a hot flow anomaly

M.O. Fillingim [a,*], J.P. Eastwood [a], G.K. Parks [a], V. Angelopoulos [b], I.R. Mann [c], S.B. Mende [a], A.T. Weatherwax [d]

[a] Space Sciences Laboratory, University of California, 7 Gauss Way, Berkeley, CA 94720-7450, USA
[b] Institute for Geophysics and Planetary Physics, University of California, Los Angeles, CA, USA
[c] Department of Physics, University of Alberta, Edmonton, Alberta, Canada
[d] Department of Physics, Siena College, Loudonville, NY, USA

ARTICLE INFO

Article history:
Accepted 1 March 2010
Available online 4 March 2010

Keywords:
Aurora
Magnetic impulse
Solar wind discontinuity
Magnetosphere/ionosphere interaction
Solar wind/magnetosphere interaction

ABSTRACT

We present observations of the ionospheric response to a hot flow anomaly (HFA) interacting with the magnetosphere. On 4 July 2007, the THEMIS spacecraft observed an HFA, a disruption of the solar wind flow, on both sides of the bow shock. The ionospheric response was measured by global auroral images taken over the southern hemisphere by Polar UVI, by ground based magnetometers and photometers in Antarctica, and by the THEMIS Ground Based Observatory (GBO) magnetometers (GMAGs) in the northern hemisphere. Polar UVI observations show a region of enhanced auroral emission in the morning sector about 10 min after the THEMIS spacecraft observed the HFA. This region of enhanced emission was located above South Pole station which observed magnetic perturbations and an increase in the auroral luminosity. The THEMIS GMAGs in the conjugate hemisphere also observed magnetic perturbations consistent with a traveling convection vortex (TCV). Polar UVI tracked the spatial and temporal development of the region of enhanced emission. Slow anti-sunward motion was observed as the emission weakened and then re-brightened over the course of about 10 min. Simultaneously, the THEMIS GMAG array observed anti-sunward motion of the magnetic impulse with a velocity much greater than that of the auroral emission. These are the first simultaneous observations of localized enhanced auroral emission and the associated magnetic impulse propagating anti-sunward over a distance of several 1000 km. We suggest that the origin of the magnetic perturbation and resulting auroral emission is the deformation of the magnetopause due to the HFA–magnetosphere interaction. The different propagation speeds of the auroral emission in the southern hemisphere and the magnetic perturbation in the northern hemisphere imply either (1) a decoupling of the auroral emission and field-aligned current signature or (2) a decoupling of these processes between the two hemispheres. The large difference in the ionospheric conductivity between the northern (summer) and southern (winter) hemispheres may be an important factor in this decoupling. More observations are needed to adequately address the decoupling mechanism.

1. Introduction

Impulsive disturbances in dayside, high-latitude, ground based magnetograms have been studied for many years. Such disturbances are important for understanding the response of the magnetosphere–ionosphere system to solar wind variability. One type of disturbance, termed as a magnetic impulse event (MIE), is characterized by impulsive deflections of the magnetic field with durations of 5–20 min and amplitudes of a few tens to a few hundreds of nT (Lanzerotti et al., 1986, 1991; Kataoka et al., 2002; Zesta et al., 2002). These events have been interpreted as the ground based signature of a pair of Hall current loops associated with traveling convection vortices (TCVs) (Friis-Christensen et al., 1988; Glassmeier et al., 1989). The TCV current system is composed of a pair of oppositely directed field-aligned currents linking the ionosphere to the dayside magnetosphere/magnetopause propagating anti-sunward at an approximately fixed magnetic latitude. Theoretical work (Southwood and Kivelson, 1990; Kivelson and Southwood, 1991) suggests that TCVs can be driven by abrupt changes in the magnetopause position due to solar wind pressure variations. Therefore, changes in the solar wind pressure are thought to lead to deformation of the magnetopause. The magnetopause deformation drives a field-aligned current system, i.e., the TCV. The MIE, then, is the ground

* Corresponding author. Tel.: +1 510 643 8485; fax: +1 510 643 8302.
E-mail address: matt@ssl.berkeley.edu (M.O. Fillingim).

1364-6826/$ - see front matter © 2010 Elsevier Ltd. All rights reserved.
doi:10.1016/j.jastp.2010.03.001

based signature of the TCV passing overhead (e.g., Glassmeier et al., 1989; Zesta et al., 2002; Sibeck et al., 2003).

Several subsequent statistical studies have attempted to determine the solar wind source of MIEs and TCVs. Sitar and Clauer (1999) found MIEs for less than half of the solar wind tangential discontinuities identified upstream of the magnetosphere. Analyzing 7 years of data, Kataoka et al. (2003) found a statistical correlation between the occurrence rate of MIEs and tangential discontinuities. However, they found over 100 times more tangential discontinuities than MIEs, suggesting that the presence of tangential discontinuities may be a necessary but not sufficient criteria for MIE generation. A more detailed analysis of a subset of MIEs with clear solar wind drivers by Kataoka et al. (2003) showed that MIEs were likely to be caused by tangential discontinuities which satisfied the criteria for the formation of hot flow anomalies (HFAs), namely an inward pointing motional electric field on at least one side of the discontinuity and a large cone angle between the tangential discontinuity normal and the Sun-Earth line (see review by Schwartz et al., 2000). Murr and Hughes (2003) were able to indentify solar wind triggers for 30 of 31 TCVs studied and found that in a majority of cases, the solar wind trigger was a foreshock cavity. Foreshock cavities are similar to HFAs in that they both cause variations in solar wind density and dynamic pressure leading to a deformation of the magnetopause (e.g., Sibeck et al., 2001). Therefore, a correlation appears to exist between MIEs/TCVs and solar wind discontinuities that lead to the development of regions of perturbed solar wind pressure (HFAs and foreshock cavities). The subsequent deformation of the magnetopause links these phenomena.

There have been very few case studies examining in detail the connection between HFAs and disturbances in ground based observations. In one well studied event (Sibeck et al., 1998, 1999; Sitar et al., 1998; Weatherwax et al., 1999), a train of TCVs was purported to be driven by an anti-sunward propagating $5R_E$ bulge on the magnetopause caused by the interaction of an HFA with the bow shock and magnetosphere. During this event, intense auroral emission was observed in the pre-noon sector in both the northern and southern hemispheres by both space-based and ground based auroral imagers.

A statistical examination of the global distribution of auroral emission (Liou et al., 1997) showed that a region of weak auroral emission is often present in the pre-noon sector centered near 09 local time. This global spatial distribution of the auroral emission was in good agreement with statistical observations of precipitating energetic electrons (Newell et al., 1996). Ground based studies also seemed to suggest a correlation between auroral emission in the pre-noon sector and either MIEs (Mende et al., 1990) or TCVs (Lühr et al., 1996). Therefore, pre-noon auroral emission may also be related to solar wind discontinuities (HFAs and foreshock cavities) interacting with the bow shock and magnetosphere.

At 10:26 UT on 4 July 2007, the THEMIS spacecraft observed an HFA interacting with the terrestrial bow shock (Eastwood et al., 2008). The THEMIS-A spacecraft, which was located just upstream of the bow shock near a local time of 14, measured a significant deflection of the plasma velocity, reduced magnetic field strength, reduced plasma density, and enhance plasma temperature. The HFA was associated with a discontinuity in the interplanetary magnetic field. Eastwood et al. (2008) also determined that the convection electric field was pointing into the discontinuity on both sides, a key formation criterion for HFAs (Schwartz et al., 2000). The reduced plasma velocity contributes to a reduced dynamic plasma pressure in the HFA. Due to this pressure change, Eastwood et al. (2008) calculated that the magnetopause should move by about $1R_E$ in the HFA–magnetopause interaction region. For a detailed analysis of this HFA event, the reader is referred to Eastwood et al. (2008).

Here we report observations of the ionospheric response to an HFA interaction with the magnetosphere. We track the ionospheric response using THEMIS Ground Based Observatory (GBO) magnetometer (GMAG) data (Mende et al., 2008; Russell et al., 2008), Antarctic magnetometer and photometer data, and global auroral images from Polar UVI (Torr et al., 1995). These observations are unprecedented in that, due to the wide spatial coverage of the THEMIS GMAGs, the magnetic and auroral signatures of the interaction can be tracked over 6 h of local time or over 3000 km in the polar ionosphere. In addition, Polar UVI was imaging the global aurora with a cadence of 36 s; in the event reported by Sitar et al. (1998) and Sibeck et al. (1999), the time between successive images taken with the same filter was over 6 min. Therefore, from both the ground and from space, we are able to follow the ionospheric response over long distances with high temporal resolution.

2. Ground based observations

Fig. 1 shows 15 min of magnetometer data from the THEMIS GMAG at Goose Bay (GBAY) in eastern Canada. At 10:40 UT, GBAY was in the pre-noon sector at a magnetic local time of 07 LT. The panels show, from top to bottom, the magnetic north (H), magnetic east (D), and vertical down (Z) components of the local magnetic field. The resolution of the data is 0.01 nT with a cadence of 2 Hz. The 30-min average is subtracted from each component, so that only the variation in the magnetic field is shown. Clear deflections in both the H and D-components of about 30 nT are seen. The H-component shows a unipolar negative deflection while the D-component exhibits a bipolar negative than positive deflection. These observations are consistent with a clockwise Hall current loop resulting from a downward field-aligned current passing north of GBAY. Assuming uniform conductivity, the ground level magnetic field caused by the parallel current is canceled by the magnetic field caused by the radial Pedersen current (the divergence of which is necessary to balance the field aligned current). At the ground, only the magnetic field caused by the Hall current is measured (e.g., Kamide and Matsushita, 1979; Glassmeier, 1987; Zesta et al., 2002). The maximum deflection in the H-component occurred at 10:37:19 UT, approximately 10 min after THEMIS-A observed the HFA signatures post-noon. Similar signatures are seen by the other THEMIS GMAGSs and by stations in Antarctica.

Earlier observations of MIE/TCV events showed that often the D-component showed a unipolar positive deflection while the H-component displayed a bipolar negative than positive displacement (approximately the negative derivative of the D-component signature) consistent with a counter-clockwise vortex followed by a clockwise vortex passing north of the stations (Glassmeier et al., 1989). However, the statistical studies of Glassmeier et al. (1989), Lanzerotti et al. (1991), and Zesta et al. (2002) showed that some MIE signatures, about 20% in the observations of Glassmeier et al. (1989), consistent of unipolar deflections of the H-component and bipolar deflections of the D-component, as is the case at GBAY and the other magnetometer stations for this event. This type of signature is consistent with a single vortex passing near the ground station. In fact, Zesta et al. (2002) found that approximately 10% of their TCV events were consistent with a single vortex rather than two or more vortices. We should note that our observations cannot preclude the possibility of more than one vortex; other much weaker vortices could be present whose signatures are indistinguishable from the background fluctuations.

Fig. 2 shows the H-component magnetograms for GBAY plus 8 other ground stations used in our analysis. The station

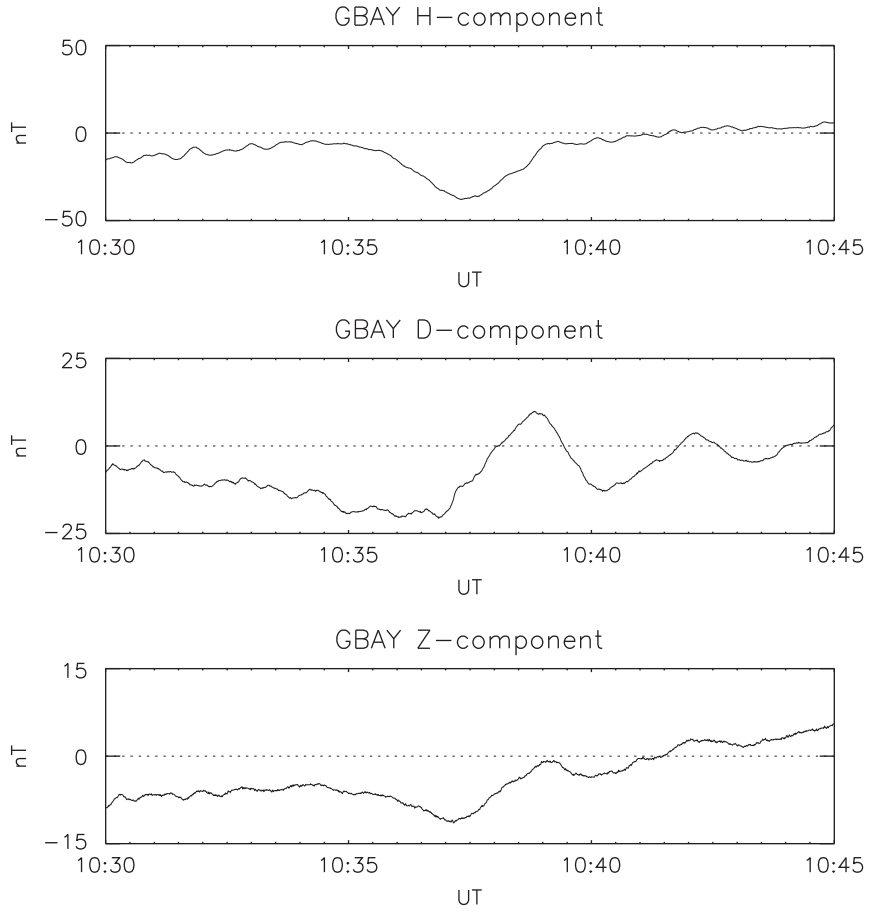

Fig. 1. From top to bottom: the magnetic north (*H*), magnetic east (*D*), and vertical down (*Z*) components of the local magnetic field observed at the THEMIS GMAG station at Goose Bay (GBAY) in eastern Canada. The 30 min average has been subtracted.

abbreviations, magnetic latitude, and magnetic local time given in magnetic apex coordinates (VanZandt et al., 1972; Richmond, 1995) are indicated on each trace. (Additionally, a map of the positions of the stations is shown in the left panel of Fig. 3.) The THEMIS GMAG stations are GBAY, CHBG, KAPU, GILL, RANK, FSMI and FSIM; the Antarctic stations are SPA and MCM, as indicated by their negative latitudes. Again, the 30 min average has been subtracted; the horizontal dotted lines indicate the zero line for each trace. The spacing between the zero lines for adjacent traces is 100 nT. The magnetograms from SPA, GILL, and RANK have been divided by 6, 2, and 2, respectively.

The magnetograms have been ordered, from top to bottom, based on the time of the maximum deflection in the *H*-component. On each trace, the time of maximum deflection in the *H*-component is indicated by the vertical dotted line. The time of maximum *H* deflection corresponds to the time when the center of the TCV is directly north (for negative deflections) or south (for positive deflections) of the station. To compute the time of maximum *H* deflection, the THEMIS GMAG data were smoothed over 1 s and the extremum of the data over the time interval of interest was determined. The times have an uncertainty of ± 0.5 s for the THEMIS GMAG data. The resolution of the Antarctic data (SPA and MCM) is 10 s, so the timing uncertainty is ± 5 s. These times are listed in Table 1 below.

Table 1 lists the location of each of the 9 ground stations in geographic latitude and longitude. The positions of the THEMIS GMAG stations were mapped to the southern hemisphere using the magnetic field model of Tsyganenko (1995) and Tsyganenko and Stern (1996) (T96) using the hourly averaged observed solar wind conditions and magnetospheric activity levels from OMNI-Web (http://omniweb.gsfc.nasa.gov). The resulting magnetic latitude and local time in the southern hemisphere are given in magnetic apex coordinates (VanZandt et al., 1972; Richmond, 1995). The magnetic local time of each station was calculated at 10:40 UT. This mapping was done in order to facilitate the organization of the data in local time and so that the positions of the stations could be shown on the UVI images (see Section 3). It should be noted that the difference in the magnetic latitude and local time in the northern hemisphere and the mapped latitude and local time in the southern hemisphere for the THEMIS GMAGs are typically quite small. The difference in magnetic latitude is about 1° or less, and, in all but one case (RANK), the difference in local time is about 0.1 h or less.

Note that in Fig. 2, SPA, MCM, and RANK show positive deflections in *H* while the remaining stations show negative deflections. This suggests that SPA, MCM, and RANK are poleward of the TCV while the remaining stations are equatorward of it. The 3 stations recording positive deflections are poleward of 72° magnetic latitude while the 6 stations recording negative deflections are equatorward of 68° latitude (see to Table 1). Therefore, the center of the TCV current system is most likely located near 70° magnetic latitude. This is also consistent with the location of the region of auroral emission (see Section 3).

It is clear that stations at later local times (closer to noon) see the MIE earlier indicating an anti-sunward propagation. One exception is South Pole Station (SPA) which sees the magnetic signature roughly 1 min later than would be anticipated by its local time position. Based on its local time, one would expect SPA

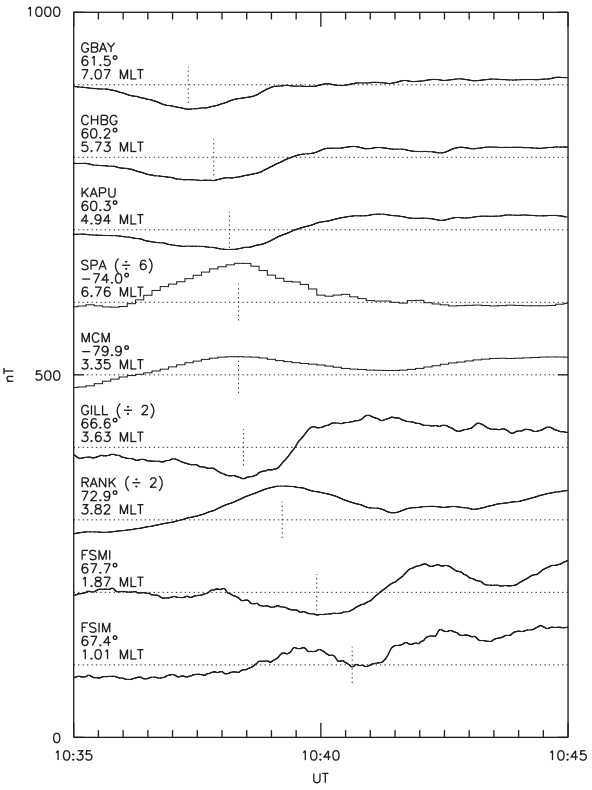

Fig. 2. The *H*-component magnetograms for the 9 ground stations used in this analysis. The 30 min average has been subtracted from each trace. The horizontal dotted line indicates the zero line for each trace. The spacing between adjacent zero lines is 100 nT. The time of maximum *H* deflection on each magnetogram is indicated by the vertical dotted line.

to see the signature between GBAY and CHBG. Another exception is Gillam Station (GILL) which sees the impulse later than McMurdo Station (MCM) which is at an earlier local time. However, the time difference between GILL and MCM is only 6 s which is near the limit of the combined uncertainties of the two instruments. A linear least-squares fit to the data gives a velocity of the magnetic signature of 1.8 h of local time per minute $\pm 20\%$ over 6 h of local time. This corresponds to a velocity of 17 ± 3 km/s over 3500 km at 70° latitude in the ionosphere.

Note that the character of the magnetic signatures is different at FSMI and FSIM, in the post-midnight sector, than at the other stations at later local times; they are not simple unipolar deflections of the *H*-component. There appears to be more structure and variation in the *H*-component at these two stations. However, we are able to identify features similar to those found in the other traces (as shown in Fig. 2) in order to perform our timing analysis. Previous studies (e.g., Lühr et al., 1996; Murr et al., 2002) have noted that the shape of the TCV current system can change as it propagates anti-sunward, starting out circular but evolving into a more elliptical and tilted shape. Such an evolution could explain the difference in the ground magnetic signature seen at FSMI and FSIM. Also, these stations are near local midnight where currents associated with nightside auroral forms and substorms can influence and add more variation to the magnetograms (see auroral observations below).

Since we assume that the field-aligned current is generated by the deformation of the magnetopause (e.g., Sibeck et al., 2003), we calculate the propagation velocity of the disturbance in the equatorial magnetosphere. To do this we map the position of the ground based stations to the equatorial plane along magnetic field lines using the T96 model. Table 2 lists the geocentric altitude of the apex of the field line emanating from each ground station as well as the *X*-component of the position of the apex and the local

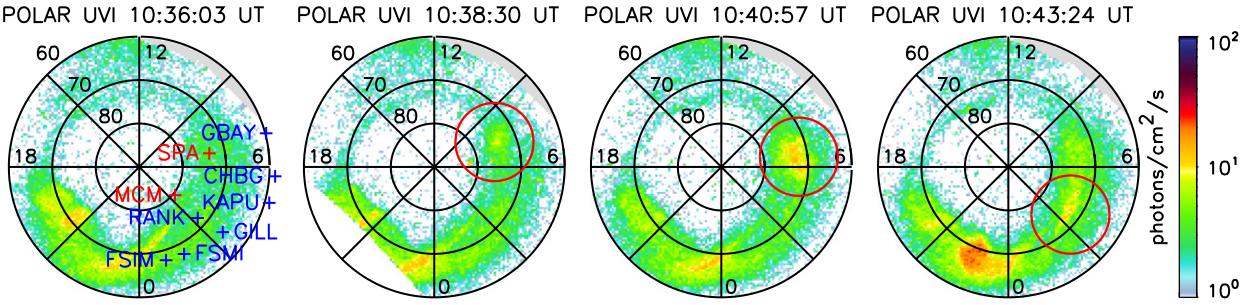

Fig. 3. A sequence of 4 global auroral images taken by the Ultraviolet Imager (UVI) onboard the Polar spacecraft over the southern hemisphere. The magnetic footprints of the ground based stations are shown on the first image.

Table 1
Summary of ground-based magnetometer observations.

Station abbreviation	Geographic latitude (°)	Geographic longitude (°)	Magnetic latitude (°)	Magnetic local time[a]	Time of maximum *H* deflection[b] (UT)
GBAY	53.32	299.5	−60.2	7.01	10:37:19
CHBG	49.81	285.6	−59.1	5.74	10:37:50
KAPU	49.39	277.7	−59.4	4.96	10:38:09
SPA[c]	−90.0	0.0	−74.0	6.76	10:38:20
MCM[c]	−77.85	166.7	−79.9	3.35	10:38:20
GILL	56.35	265.3	−66.0	3.43	10:38:26
RANK	62.83	267.9	−72.5	3.20	10:39:13
FSMI	59.98	248.2	−67.7	1.75	10:39:55
FSIM	61.76	238.8	−67.8	1.00	10:40:38

[a] Magnetic local time at 10:40:00 UT.
[b] Times for THEMIS GMAGs are ± 0.5 s; times for Antarctic stations are ± 5 s.
[c] Antarctic stations.

Table 2
Summary of ground based observations mapped to the equatorial plane.

Station abbreviation	Geocentric radius of apex (R_E)	X-Component of apex (R_E)	Local time of apex[a]	Time of maximum H deflection (UT)
GBAY	4.46	1.12	6.97	10:37:19
CHBG	4.12	−0.24	5.77	10:37:50
KAPU	4.19	−1.10	4.98	10:38:09
SPA	14.56	−3.22	5.14	10:38:20
GILL	8.02	−4.74	3.53	10:38:26
RANK	20.76	−16.87	2.37	10:39:13
FSMI	12.18	−10.91	1.53	10:39:55
FSIM	14.54	−13.91	0.76	10:40:38

[a] Local time is calculated at 10:40:00 UT in GSM coordinates.

time of the apex in GSM coordinates at 10:40 UT. The field line from MCM extended more than $70R_E$ down tail out of the valid region of the model, so its apex position could not be determined; hence it is not listed in Table 2.

The local time of the apex of the field line is not significantly different from the local time of the ground station in most cases. South Pole Station (SPA) is a notable exception. The local time of the station is 6.76 while the local time of the apex of its magnetic field line is 5.14, a shift of over 1.5 h. The local time of the apex of the SPA field line is very close to the local time KAPU (however, the apexes of the field lines are separated by $10R_E$ in the Y-direction). The time discrepancy between SPA and the other stations of about 1 min noted above based on the station local times is now reduced to about 10 s if the local time of the apex of the field line is considered.

The least-squares fit velocity using the local times of the field line apexes is 1.9 h of local time per minute $\pm 10\%$. This velocity is virtually identical to the 1.8 h/min determined from the ground local time positions; however, there is less spread in the data leading to a smaller uncertainty (10% versus 20%).

We now consider the X velocity of the disturbance by performing a least squares fit to the X-component of the apex of the field lines listed in Table 2. We find a propagation velocity of $325R_E$/h $\pm 25\%$ or 575 ± 140 km/s in the negative X-direction (anti-sunward). This velocity is comparable to the 600 km/s solar wind velocity observed by THEMIS-A outside the HFA (Eastwood et al., 2008) and other upstream monitors. Along the dawn flank of the magnetopause, the deformation should propagate with the magnetosheath speed (which, along the dawn flank, is also nearly equal to the solar wind speed). This suggests that the speed of propagation of the magnetic disturbance is determined by the speed at which the HFA-bow shock–magnetopause interaction region moves down the dawn flank.

3. Polar UVI observations

Fig. 3 shows a sequence of four global auroral images taken by the Ultraviolet Imager (UVI) onboard the Polar spacecraft near apogee at $9R_E$ above the southern hemisphere. The images in Fig. 3 are integrated over 37 s and are separated by about two and a half minutes (however, UVI recorded an image every 37 s). The time at the top of each image is the beginning of the 37 s integration period. These images were taken with a filter which is sensitive to Lyman–Birge–Hopfield (LBH) emissions in the wavelength range from 160 to 180 nm. These emissions are primarily produced by electron impact on N_2, and the intensity of the emission is directly proportional to the precipitating electron energy flux (Germany et al., 1997). The image data have been transformed into magnetic apex coordinates. The image projection is such that the observer is looking through Earth from above the north pole. A line-of-sight correction, compensating for the increased emission due to the longer path length through the atmosphere for slant viewing as compared to nadir viewing, has been applied to these images.

The first image shows only diffuse, low level emission on the dayside. Also plotted on the first image are the locations of the ground based stations listed in Table 1. The stations in red are the Antarctic stations; the stations in blue are the northern hemisphere THEMIS GMAGs mapped to the southern hemisphere. The aurora begins to brighten at 10:38:30 UT near 08 MLT at a latitude of $\sim 75^\circ$ as circled in the second image. (The white region in the second image between 18 and 24 MLT at latitudes less than 70° is missing data.) Two and a half minutes later, in the third image, the aurora has brightened significantly, the region of enhanced emission has grown in latitude and local time, and the emission has moved anti-sunward to about 07 MLT. In the fourth image, the emission in the pre-noon sector has decreased to pre-event levels while the region of enhanced emission has moved past dawn to about 04 MLT. It should be noted that the Polar spacecraft "wobble" is approximately in the 09–21 magnetic local time (MLT) direction at this time. The effect of the wobble is such that it exaggerates the latitudinal extent of the emission region in the third image and exaggerates the local time extent of this region in the last image.

The initial auroral brightening in the UVI images appears above South Pole Station (SPA). Using the 10-s resolution photometer data from SPA, we can more accurately determine the timing of the onset of the brightening. Fig. 4 shows the auroral intensity at 630.0 and 427.8 nm from SPA and the auroral intensity from the UVI images summed over latitudes from 65° to 80° and local times from 03 to 09 MLT. The vertical dashed lines mark the beginning and ending times of the 37-s integration period of the UVI image during which the brightening is first seen: 10:38:30–10:39:07 UT. The time of initial brightening is consistent among all three instruments at about 10:38:45 UT.

The time delay between the maximum H deflection at SPA (10:38:20 UT) and the time of the beginning of the auroral brightening at SPA is about 20–30 s. The time delay between the maximum H deflection at SPA and maximum auroral intensity at SPA (10:40:00 UT) is about 100 s.

The integrated peak intensity observed by UVI occurs between 10:40:57 and 10:41:34 UT (the third image in Fig. 3), approximately 60–90 s later than the peak intensity observed at SPA at both 630.0 and 427.8 nm. This is most likely due to the fact that the region of emission covers an area of the ionosphere larger than the photometer field of view. This means that while the intensity of the emission may have reached its maximum as seen by the photometers, the region of emission continues to expand as measured by the integrated intensity (intensity times area) observed by UVI.

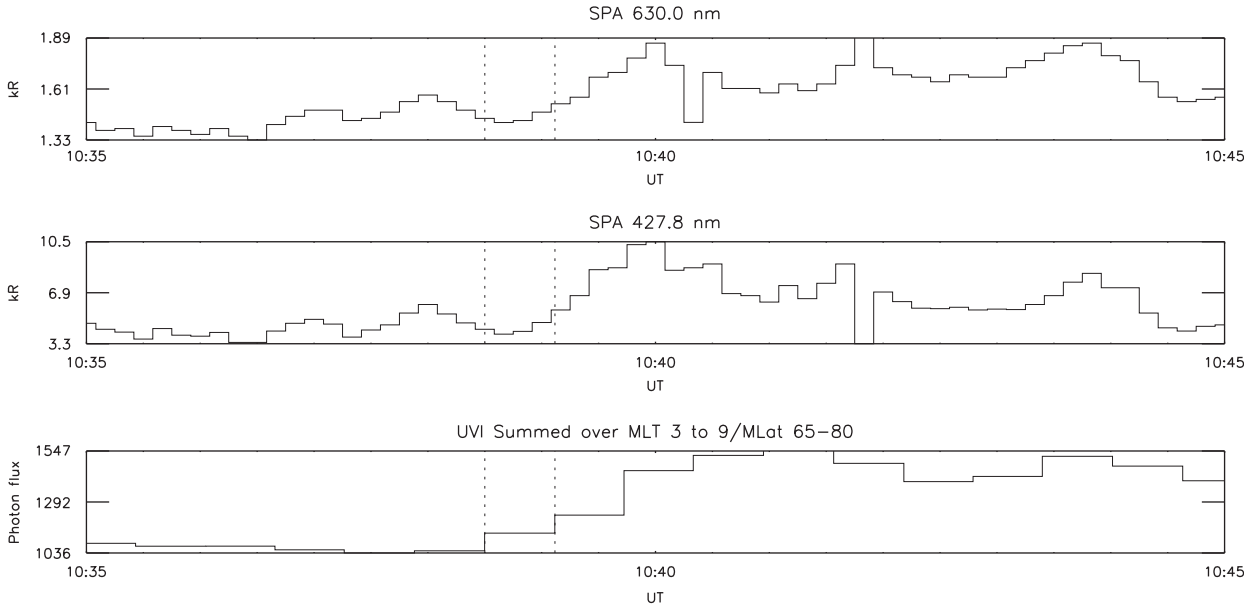

Fig. 4. Auroral intensity at 630.0 nm (top panel) and 427.8 nm (second panel) observed by South Pole (SPA) photometers. Auroral intensity summed over magnetic local times from 03 to 09 and magnetic latitudes from 65° to 80° observed by UVI (bottom panel). The vertical dashed lines demark the UVI integration period when the increase in auroral emission begins.

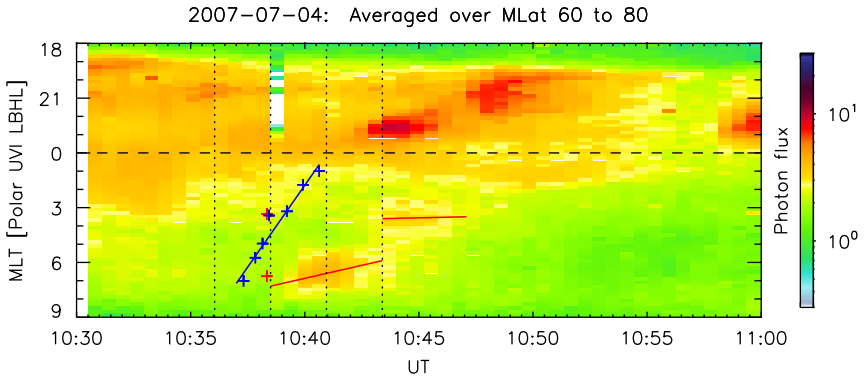

Fig. 5. Auroral intensity as a function of Universal Time and magnetic local time averaged over magnetic latitudes from 60° to 80° as observed by UVI. The plus signs show the Universal Times and magnetic local times of the maximum *H* deflections as observed by the ground based stations. The lines show the propagation speeds of the magnetic disturbance (blue) and the region of auroral emission (red).

By binning the auroral image data into 1° magnetic latitude bins and 0.2 h MLT bins, we can construct an MLT keogram as shown in Fig. 5. This keogram shows the auroral intensity as a function of UT and MLT averaged over a fixed latitude range, 60°–80° magnetic latitude in this case. Also shown on the keogram are the times of the maximum *H* deflection observed by the ground based magnetometers and the MLT locations of the stations as given in Table 1. The times and locations for the northern hemisphere THEMIS GMAG stations are represented by the blue pluses; the times and locations for the Antarctic stations are represented by the red pluses. The least-squares fit line is also shown (blue line). The vertical dotted lines show the times of the images shown in Fig. 3.

The dayside auroral brightening is seen near the bottom of the keogram at local times of ~06 MLT around 10:40 UT. The red lines show the average propagation speeds of the maximum auroral intensity observed by UVI. The average propagation speed of the region of enhanced emission from 10:38:30 to 10:43:24 UT is 0.29 h of MLT per minute over 1.4 h of local time. At 70° latitude, this corresponds to an anti-sunward speed of ~2.7 km/s in the ionosphere, over six times slower than the propagation speed of the magnetic impulse computed above. At 10:43:24 UT, there appears to be a jump of the location of the maximum of the emission from 06 MLT to about 3.5 MLT. From 10:43:24 to 10:47:05 UT, the region of auroral emission is nearly stationary; the propagation speed of the auroral emission is about 0.027 h/min, an order of magnitude slower than its earlier speed.

It is interesting to note that there is a sudden brightening of the aurora on the night side near 23 MLT at 10:42:47 UT. This is the brightening of a region of pre-existing emission (see Fig. 3). The timing of this brightening appears to coincide with the arrival of the magnetic impulse signature to this local time; i.e., the propagation velocity of the magnetic signature (blue line) reaches 23 MLT at about the time the aurora brightens. We leave open the possibility that the magnetic disturbance initiated a substorm once it reached the night side.

4. Discussion

The event described here is only the second well documented observation of the large scale auroral response to an HFA. Our

event shares several similarities with the previous event reported by Sitar et al. (1998), Sibeck et al. (1999), and Weatherwax et al. (1999), but it also contains some important differences. In both events, a magnetic impulse consistent with the signature of a TCV is observed in response to the HFA interacting with the bow shock and magnetopause. The field-aligned current that characterizes the TCV is presumably driven by the deformation of the magnetopause resulting from the low pressure region of the HFA interacting with the magnetopause (e.g., Cowley, 2000; Sibeck et al., 2000). Also, shortly after the magnetic signature, a significant brightening of the pre-noon aurora is observed.

The time delay between the HFA observations by THEMIS-A at 10:26 UT near 14 MLT and the magnetic deflection measured at GBAY at 10:37 UT at 07 MLT is about 11 min. Using our calculated TCV velocity of 1.8 h of local time per minute, one could expect the disturbance to traverse the 7 h of local time from the THEMIS-A observations to GBAY in less than 4 min. However, our velocity determinations were made in the dawn/pre-dawn sector where the propagation speed along the magnetopause should approach the magnetosheath/solar wind speed. Straightforward geometrical arguments show that, for a structure at an oblique angle with respect to the Sun-Earth line, the propagation along the magnetopause from the dusk sector, across local noon, and toward the dawn sector should be much slower than the solar wind velocity. This velocity depends upon two angles: the angle between the normal to the structure (the tangential discontinuity giving rise to the HFA) and the solar wind velocity which is fixed and the angle between the discontinuity and the normal to the magnetopause which changes as the discontinuity propagates along the magnetopause. As the angle between the normal to the discontinuity and the solar wind velocity increases, the velocity across the nose of the magnetopause decreases. For example, for a discontinuity-solar wind velocity angle $>60^{\circ}$, the propagation along the nose of the magnetopause is <0.5 the solar wind velocity. From the presence of foreshock wave activity, Eastwood et al. (2008) were able to determine that the discontinuity was at an oblique angle to the Sun-Earth line (i.e., quasi-parallel); the exact angle was not measured, however. It is clear, then, that we should expect the time delay between the THEMIS-A and GBAY observations to be significantly longer than 4 min.

The observations of Sitar et al. (1998) and Sibeck et al. (1999) showed that, in the same local time sector, the time delay between HFA observations and strong ground magnetic deflections was about 3 min. For a more recent event, Jacobsen et al. (2009) showed that the time delay between THEMIS observations of an HFA on the dawn side magnetosphere and ground signatures of an MIE/TCV in the same local time sector was about 2 min. Therefore, in addition to the propagation along the magnetopause, there appears to be a 2–3 min time delay from the magnetopause to the ionosphere. Taken together then, a time delay of 11 min from HFA observation in the dusk sector to ground signatures in the dawn sector is not unreasonable.

Sitar et al. (1998) reported that there was a 10 min delay between the magnetic signature detected on the ground and the brightening of the aurora at similar local times. However, their observations were complicated by the fact that several magnetic impulses were seen for 45 min prior to one that was associated with the aurora. In fact, the time delay between the most intense magnetic deflection and the increase in auroral emission was about 2 min. Given the coarse temporal resolution of the UVI data for the previous event, the time delay may have been even shorter. For the same event, Weatherwax et al. (1999) reported essentially no time delay between the maximum H deflection and the onset of auroral brightening as observed by magnetometers and photometers at South Pole station (SPA). For our event, the delay time between the initial maximum H deflection observed at GBAY (10:37:19 UT) in the northern hemisphere and the initial brightening of the aurora seen by UVI (10:38:45 UT) in the southern hemisphere is about 90 s. The time delay between the maximum H deflection and the auroral brightening using only Antarctic data from SPA, rather than a comparison between northern and southern hemisphere data, is about 30 s, consistent with the earlier results of Weatherwax et al. (1999).

For our event, the calculated propagation speed of the TCV in the ionosphere over 6 h of local time is about 17 km/s. Early TCV observations (e.g., Friis-Christensen et al., 1988; Glassmeier et al., 1989) suggested a typical speed of 2–4 km/s. A large statistical study of TCV properties by Zesta et al. (2002) found propagation velocities typically between 3 and 11 km/s with a mean near 8 km/s. However, they reported propagation velocities up to 20 km/s. Jacobsen et al. (2009) recently reported observations of a MIE/TCV event with a velocity of $\sim$25 km/s. In a well-observed case study, Lühr et al. (1996) reported that the propagation velocity of a TCV increased from about 2.5 km/s to nearly 8 km/s as the TCV traveled from noon to dawn. So not only is there a wide range in TCV velocities, but they may also accelerate as they propagate. Our analysis, specifically the blue, best-fit line on Fig. 5, does not indicate significant acceleration.

For the previous event, Sitar et al. (1998) computed a TCV propagation speed of 9.7 km/s. Interestingly, for the same event studied by Sitar et al. (1998), Weatherwax et al. (1999) determined a propagation velocity of $\sim$3 km/s for the TCV using Antarctic magnetometer data. If the TCV propagation velocity is tied to the propagation velocity of the deformation of the magnetopause as it is swept down tail, then one may expect the TCV speed to depend upon the magnetosheath or solar wind speed. For our event, as noted above, the solar wind velocity was over 600 km/s. Both Sitar et al. (1998) and Sibeck et al. (1999) reported that the solar wind velocity was just over 350 km/s during the previous event. The difference in propagation velocities ($17/10=1.7$) compares favorably with the difference in solar wind speeds ($600/350=1.7$) for the two events.

The duration of the MIE/TCV signatures at GBAY (Fig. 1) and the other ground based stations (Fig. 2), is about 3–4 min. At a velocity of 17 km/s, this yields a spatial extent of 3000–4000 km. This size is in general agreement with the statistical results of Zesta et al. (2002) which yielded a characteristic size of $\sim$3000 km. Our size estimate translates to $\sim$5–7 h of local time at 70° latitude or to $\sim 80^{\circ}$–100° longitude.

Sitar et al. (1998) noted that the duration of the auroral emission during the previous event was about 18 min and, at its maximum extent, covered 5° in latitude (500 km) and 4 h in MLT centered at 75° latitude (1700 km). In our event, the duration of the enhanced auroral emission is shorter, just over 8 min, and the region of emission covers 5° in latitude (500 km) and 3 h in MLT centered around 70° latitude (1700 km) at its maximum extent. The region of emission in our event covers fewer hours of local time, but the equatorial shift of the region of emission results in roughly the same spatial extent for both events. The longitudinal size of the region of auroral emission is about half the longitudinal size of the MIE/TCV signature.

The maximum intensity of the auroral emission during our event is less than that seen by UVI during the previous event by about a factor of 2. We interpret this observation to suggest that the causative agent (the magnetopause deformation) was stronger during the previous event than the current one. Sibeck et al. (1999) observed the magnetopause deformation to be about $5R_E$ in the pre-noon sector. Based on the pressure decrease in the HFA as measured by THEMIS-A, Eastwood et al. (2008) calculated a magnetopause perturbation of approximately $1R_E$, consistent with the idea that our event is weaker because the magnetopause deformation is less. The shorter duration of our event compared to

the event of Sitar et al. (1998), 8 min versus 18 min, could be due to either the faster propagation speed (the disturbance moves down the dawn flank faster) or due to the smaller deformation of the magnetopause (the smaller deformation may be shorter lived).

The coarse, 6-min temporal resolution of the UVI images during the previous event did not allow for an effective determination of the propagation velocity of the region of auroral emission. The higher cadence, 36-s UVI data available for our event have allowed us to track the development and motion of the region of emission. We find that the auroral emission propagates anti-sunward at about 3 km/s, about 6 times slower than the TCV. The TCV velocity was determined using mainly (7 out of 9) northern (summer) hemisphere ground stations. Even if we remove the two southern hemisphere stations, the TCV propagation velocity is unchanged. The auroral propagation velocity was determined using southern (winter) hemisphere UVI observations. As mentioned above, Sitar et al. (1998) computed a TCV velocity of nearly 10 km/s in the northern hemisphere for the previous event while Weatherwax et al. (1999) computed a velocity of about 3 km/s in the southern hemisphere. The previous event also occurred near northern summer solstice (24 July 1996). In both cases, the winter (southern) hemisphere velocity was slower than the summer (northern) hemisphere velocity. This suggests that the difference in velocity between the magnetic and auroral signature could be due to a hemispheric effect.

The ionospheric conductivity is significantly different between the summer and winter hemispheres. The higher ambient conductivity in the summer hemisphere could allow the current system associated with the TCV to be more easily driven and close through the ionosphere. In the winter hemisphere, the conductivity may be insufficient to support the imposed currents. Potentials must then be set up to accelerate precipitating particles in order to increase the ionospheric conductivity. The time needed to form the potentials and increase the conductivity may slow the propagation of the current system.

Alternatively, the difference in velocity between the magnetic and auroral signature may be due a decoupling of the auroral emission from the TCV current system. Sitar et al. (1998) interpreted the region of auroral emission observed during the previous event as the footprint of an upward field-aligned current with the precipitating electrons carrying the upward current. However, rather than a downward–upward field-aligned current pair as Sitar et al. (1998) observed, our observations are more consistent with a single downward field aligned current. Normally, one would not expect strong auroral emission associated with a downward field-aligned current, i.e., upward traveling electrons. As mentioned above, we cannot preclude the presence of an upward field-aligned current component to the TCV provided its magnetic signatures are sufficiently weak. However, we would not expect such a weak current to be capable of producing a region of enhanced auroral emission.

Lühr et al. (1996) reported on a TCV event and the associated auroral emission from ground based all sky camera data. The auroral intensity brightened as the TCV current system passed overhead. While the current system continued to propagate at a speed of several km/s anti-sunward, the region of auroral emission brightened and expanded, but the center of the emission region remained stationary. Instead of interpreting the emission as the ionospheric footprint of the current system, they concluded that the TCV triggered an energetic precipitation event when it passed through a metastable region of the magnetosphere magnetically conjugate to their observations. The mechanism or instability by which the auroral precipitation could occur was not addressed. However, such a picture could also explain the apparent jump in the auroral emission at ~10:43 UT from 06 to 3.5 MLT. If the TCV current system passed through two metastable regions in the magnetosphere, two regions of auroral emission may develop at different locations not necessarily with an obvious direct connection between them.

5. Conclusions

Using a large spatial array of ground magnetometers in conjunction with global auroral images, we investigate the ionospheric response to the interaction of a HFA with the magnetosphere. A magnetic impulse consistent with the signature of a TCV is observed by the magnetometers to travel anti-sunward from pre-noon to post-midnight local times. The speed and direction of propagation of the magnetic disturbance is consistent with that of HFA–magnetopause interaction region traveling along the dawn flank at approximately the solar wind speed.

Approximately 1 min after the maximum magnetic disturbance, the auroral emission in the pre-noon sector significantly increased. The region of intense auroral emission expanded in latitude and local time and moved slowly anti-sunward over the next several minutes. The propagation velocity of the region of auroral emission was 6 times slower than that of the magnetic disturbance. Therefore, either there is a decoupling of the auroral emission from the TCV current system, or, since the auroral observations are made in the southern (winter) hemisphere and most of the magnetometer stations are in the northern (summer) hemisphere, there is a decoupling of these processes between the two hemispheres. The large difference in the ionospheric conductivity between the two hemispheres may be an important factor in this decoupling. Further conjugate observations of MIEs/TCVs and auroral emission are needed to adequately address this issue.

Acknowledgments

This work was supported in part by NASA Grant NAG5-11416. The THEMIS Mission is supported by NASA Contract NAS5-02099. We thank C.T. Russell for use of the GMAG data and the CSA for support of the CARISMA network.

References

Cowley, S.W.H., 2000. Magnetosphere–ionosphere interactions: a tutorial review. In: Ohtani, S., Fujii, R., Hesse, M., Lysak, R.L. (Eds.), Magnetospheric Current Systems. American Geophysical Union, Washington, DC, pp. 91–106.

Eastwood, J.P., Sibeck, D.G., Angelopoulos, V., Phan, T.D., Bale, S.D., McFadden, J.P., Cully, C.M., Mende, S.B., Larson, D., Frey, S., Carlson, C.W., Glassmeier, K.-H., Auster, H.U., Roux, A., Le Contel, O., 2008. THEMIS observations of a hot flow anomaly: solar wind, magnetosheath, and ground-based measurements. Geophysical Research Letters 35, L17S03, doi:10.1029/2008GL033475.

Friis-Christensen, E., McHenry, M.A., Clauer, C.R., Vennerstrøm, S., 1988. Ionospheric traveling convection vortices observed near the polar cleft: a triggered response to sudden changes in the solar wind. Geophysical Research Letters 15 (3), 253–256.

Germany, G.A., Parks, G.K., Brittnacher, M., Cumnock, J., Lummerzheim, D., Spann, J.F., Chen, L., Richards, P.G., Rich, F.J., 1997. Remote determination of auroral energy characteristics during substorm activity. Geophysical Research Letters 24 (8), 995–998.

Glassmeier, K.-H., 1987. Ground-based observations of field-aligned currents in the auroral zone: methods and results. Annales Geophysicae 5 (6), 115–126.

Glassmeier, K.-H., Hönisch, M., Untiedt, J., 1989. Ground-based and satellite observations of traveling magnetospheric convection twin vortices. Journal of Geophysical Research 94 (A3), 2520–2528.

Jacobsen, K.S., Phan, T.D., Eastwood, J.P., Sibeck, D.G., Moen, J.I., Angelopoulos, V., McFadden, J.P., Engebretson, M.J., Provan, G., Larson, D., Fornaçon, K.-H., 2009. THEMIS observations of extreme magnetopause motion caused by a hot flow anomaly. Journal of Geophysical Research 114, A08210, doi:10.1029/2008JA013873.

Kamide, Y., Matsushita, S., 1979. Simulation studies of ionospheric electric fields and currents in relation to field-aligned currents, 1, Quiet periods. Journal of Geophysical Research 84 (A8), 4083–4098.

Kataoka, R., Fukunishi, H., Lanzerotti, L.J., Rosenberg, T.J., Weatherwax, A.T., Engebretson, M.J., Watermann, J., 2002. Traveling convection vortices induced by solar wind tangential discontinuities. Journal of Geophysical Research 107 (A12), 1455, doi:10.1029/2002JA009459.

Kataoka, R., Fukunishi, H., Lanzerotti, L.J., 2003. Statistical identification of solar wind origins of magnetic impulse events. Journal of Geophysical Research 108 (A12), 1436, doi:10.1029/2003JA010202.

Kivelson, M.G., Southwood, D.J., 1991. Ionospheric traveling vortex generation by solar wind buffeting of the magnetosphere. Journal of Geophysical Research 96 (A2), 1661–1667.

Lanzerotti, L.J., Lee, L.C., Maclennan, C.G., Wolfe, A., Medford, L.V., 1986. Possible evidence of flux transfer events in the polar ionosphere. Geophysical Research Letters 13 (11), 1089–1092.

Lanzerotti, L.J., Konik, R.M., Wolfe, A., Venkatesan, D., Maclennan, C.G., 1991. Cusp latitude magnetic impulse events 1. Occurrence statistics. Journal of Geophysical Research 96 (A8), 14009–14022.

Liou, K., Newell, P.T., Meng, C.-I., Brittnacher, M., Parks, G., 1997. Synoptic auroral distribution: a survey using Polar ultraviolet imagery. Journal of Geophysical Research 102 (A12), 27197–27205.

Lühr, H., Lockwood, M., Sandholt, P.E., Hansen, T.L., Moretto, T., 1996. Multi-instrument ground-based observations of a travelling convection vortices event. Annales Geophysicae 14 (2), 162–181.

Mende, S.B., Rairden, R.L., Lanzerotti, L.J., Maclennan, C.G., 1990. Magnetic impulses and associated optical signatures in the dayside aurora. Geophysical Research Letters 17 (2), 131–134.

Mende, S.B., Harris, S.E., Frey, H.U., Angelopoulos, V., Russell, C.T., Donovan, E., Jackel, B., Greffen, M., Peticolas, L.M., 2008. The THEMIS array of ground-based observatories for the study of auroral aubstorms. Space Science Reviews 141 (1–4), 357–387.

Murr, D.L., Hughes, W.J., 2003. Solar wind drivers of traveling convection vortices. Geophysical Research Letters 30 (7), 1354, doi:10.1029/2002GL015498.

Murr, D.L., Hughes, W.J., Rodger, A.S., Zesta, E., Frey, H.U., Weatherwax, A.T., 2002. Conjugate observations of traveling convection vortices: the field-aligned current system. Journal of Geophysical Research 107 (A10), 1306, doi:10.1029/2002JA009456.

Newell, P.T., Lyons, K.M., Meng, C.-I., 1996. A large survey of electron acceleration events. Journal of Geophysical Research 101 (A2), 2599–2614.

Richmond, A.D., 1995. Ionospheric electrodynamics using magnetic apex coordinates. Journal of Geomagnetism and Geoelectricity 47 (2), 191–212.

Russell, C.T., Chi, P.J., Dearborn, D.J., Ge, Y.S., Kuo-Tiong, B., Means, J.D., Pierce, D.R., Rowe, K.M., Snare, R.C., 2008. THEMIS Ground-Based Magnetometers. Space Science Reviews 141 (1–4), 389–412.

Schwartz, S.J., Paschmann, G., Sckopke, N., Bauer, T.M., Dunlop, M., Fazakerley, A.N., Thomsen, M.F., 2000. Conditions for the formation of hot flow anomalies at Earth's bow shock. Journal of Geophysical Research 105 (A6), 12639–12650.

Sibeck, D.G., Borodkova, N.L., Zastenker, G.N., Romanov, S.A., Sauvaud, J.-A., 1998. Gross deformation of the dayside magnetopause. Geophysical Research Letters 25 (4), 453–456.

Sibeck, D.G., Borodkova, N.L., Schwartz, S.J., Owen, C.J., Kessel, R., Kokubun, S., Lepping, R.P., Lin, R., Liou, K., Lühr, H., McEntire, R.W., Meng, C.-I., Mukai, T., Nemecek, Z., Parks, G., Phan, T.D., Romanov, S.A., Safrankova, J., Sauvaud, J.-A., Singer, H.J., Solovyev, S.I., Szabo, A., Takahashi, K., Williams, D.J., Yumoto, K., Zastenker, G.N., 1999. Comprehensive study of the magnetospheric response to a hot flow anomaly. Journal of Geophysical Research 104 (A3), 4577–4593.

Sibeck, D.G., Kudela, K., Lepping, R.P., Lin, R., Nemecek, Z., Nozdrachev, M.N., Phan, T.-D., Prech, L., Safrankova, J., Singer, H., Yermolaev, Y., 2000. Magnetopause motion driven by interplanetary magnetic field variations. Journal of Geophysical Research 105 (A11), 25155–25169.

Sibeck, D.G., Decker, R.B., Mitchell, D.G., Lazarus, A.J., Lepping, R.P., Szabo, A., 2001. Solar wind preconditioning in the flank foreshock: IMP 8 observations. Journal of Geophysical Research 106 (A10), 21675–21688.

Sibeck, D.G., Trivedi, N.B., Zesta, E., Decker, R.B., Singer, H.J., Szabo, A., Tachihara, H., Watermann, J., 2003. Pressure–pulse interaction with the magnetosphere and ionosphere. Journal of Geophysical Research 108 (A2), 1095, doi:10.1029/2002JA009675.

Sitar, R.J., Clauer, C.R., 1999. Ground magnetic response to sudden changes in the interplanetary magnetic field orientation. Journal of Geophysical Research 104 (A12), 28343–28350.

Sitar, R.J., Baker, J.B., Clauer, C.R., Ridley, A.J., Cumnock, J.A., Papitashvili, V.O., Spann, J., Brittnacher, M.J., Parks, G.K., 1998. Multi-instrument analysis of the ionospheric signatures of a hot flow anomaly occurring on July 24, 1996. Journal of Geophysical Research 103 (A10), 23357–23372.

Southwood, D.J., Kivelson, M.G., 1990. The magnetohydrodynamic response of the magnetospheric cavity to changes in solar wind pressure. Journal of Geophysical Research 95 (A3), 2301–2309.

Torr, M.R., Torr, D.G., Zukic, M., Johnson, R.B., Ajello, J., Banks, P., Clark, K., Cole, K., Keffer, C., Parks, G., Tsurutani, B., Spann, J., 1995. A far ultraviolet imager for the international solar-terrestrial physics mission. Space Science Reviews 71 (1–4), 329–383.

Tsyganenko, N.A., 1995. Modeling the Earth's magnetospheric magnetic field confined within a realistic magnetopause. Journal of Geophysical Research 100 (A4), 5599–5612.

Tsyganenko, N.A., Stern, D.P., 1996. Modeling the global magnetic field of the large-scale Birkeland current systems. Journal of Geophysical Research 101 (A12), 27187–27198.

VanZandt, T.E., Clark, W.L., Warnock, J.M., 1972. Magnetic apex coordinates: a magnetic coordinate system for the ionospheric F_2 layer. Journal of Geophysical Research 77 (13), 2406–2411.

Weatherwax, A.T., Vo, H.B., Rosenberg, T.J., Mende, S.B., Frey, H.U., Lanzerotti, L.J., Maclennan, C.G., 1999. A dayside ionospheric absorption perturbation in response to a large deformation of the magnetopause. Geophysical Research Letters 26 (4), 517–520.

Zesta, E., Hughes, W.J., Engebretson, M.J., 2002. A statistical study of traveling convection vortices using the Magnetometer Array for Cusp and Cleft Studies. Journal of Geophysical Research 107 (A10), 1317, doi:10.1029/1999JA000386.